Colloids and Surfaces B: Biointerfaces 253 (2025) 114757

Contents lists available at ScienceDirect

Colloids and Surfaces B: Biointerfaces

journal homepage: www.elsevier.com/locate/colsurfb

Precision surface-immobilized peptide on graphene/chitosan composite sponge for rapid hemostasis of uncontrolled bleeding

Fanglin Du [a,1], Yuanhang Wang [a,1], Wengjing A [a], Muyuan Tang [a], Fang Liu [b], Xiaojiao Pan [c,*], Xing Wang [a,*], Guofeng Li [a,*]

[a] State Key Laboratory of Organic-Inorganic Composites, Beijing Laboratory of Biomedical Materials, Beijing University of Chemical Technology, Beijing 100029, China
[b] Department of Oncology of Integrative Chinese and Western Medicine, China-Japan Friendship Hospital, Beijing 100029, China
[c] Dezhou Women and Children's Hospital, Dezhou 253000, China

ARTICLE INFO

Keywords:
Hemostasis
Graphene/chitosan composite
Thrombin receptor-activating peptide (TRAP)
Thiol-ene photoclick chemistry
Synergistic hemostasis

ABSTRACT

Efficient and safe hemostasis for trauma-induced bleeding remains a critical challenge. In this study, we developed a peptide-immobilized graphene/chitosan composite sponge (GCCS-TRAP) for enhanced hemostatic performance. The thrombin receptor-activating peptide (TRAP) was precisely immobilized on the surface of a graphene/chitosan crosslinked sponge via thiol-ene photoclick chemistry. GCCS-TRAP exhibited outstanding liquid absorption capabilities, absorbing up to 30 times its own weight with a rapid absorption rate of 0.27 seconds. The sponge also demonstrated remarkable mechanical strength of 96.3 kPa. More importantly, GCCS-TRAP effectively activated platelets and the coagulation cascade, showing superior *in vitro* coagulation properties with a blood coagulation index of 7.1 %. In a rat femoral artery hemorrhage model, GCCS-TRAP achieved rapid hemostasis within 81.3 seconds, reducing blood loss by up to 62 % compared to commercial hemostatic materials such as chitosan-based powders, gelatin-based sponge, and polysaccharide-based powders. Additionally, GCCS-TRAP exhibited excellent biocompatibility, with minimal hemolysis and cytotoxicity. This innovative strategy of peptide immobilization via light-controlled chemistry offers a promising approach to designing next-generation hemostatic agents, optimizing peptide usage while maximizing hemostatic efficacy and safety.

1. Introduction

Trauma-induced bleeding is a common occurrence in both everyday life and on the battlefield. Severe bleeding can lead to complications such as hypothermia, hypotension, organ failure, hemorrhagic shock, and even death[1–3]. Uncontrolled bleeding, in fact, remains the leading cause of trauma-related fatalities, with a mortality rate reaching up to 50 %[4,5].

Over the past few decades, various hemostatic materials have been developed to address uncontrolled bleeding[6–15]. Polysaccharides, such as oxidized cellulose and starch, promote hemostasis by absorbing plasma at the wound site, rapidly aggregating blood cells and platelets [16,17]. Inorganic materials, like kaolin and montmorillonite, facilitate hemostasis through the synergistic effects of blood absorption and coagulation cascade activation[18–20]. In contrast, bioactive compounds, such as fibrinogen and thrombin, possess stronger coagulation properties that promote clotting by activating platelets or the coagulation cascade[21–23]. To further enhance hemostatic capacity, clotting peptides have gained significant attention. For instance, snake venom peptides, such as hemocoagulase (reptilase), are used to treat both internal and external bleeding[24,25]. Clotting is rapidly initiated even at their nanomolar concentrations due to the potent action in inhibiting plasminogen activator, releasing tissue factors, and enhancing platelet adhesion and aggregation[26]. Additionally, thrombin receptor-activating peptide-6 (TRAP), corresponding to amino acids 42–47 of the thrombin receptor, has been shown to induce platelet aggregation by activating the PAR-1 receptor on platelets[27–30]. However, the strong coagulation activity of these peptides can lead to severe thrombosis, including deep vein thrombosis (DVT), pulmonary embolism, cerebral embolism, and infarction[31]. Therefore, it is crucial to fully harness the hemostatic potential of these peptides while mitigating their toxic side effects.

* Corresponding authors.
E-mail addresses: panxiaojiao0273@163.com (X. Pan), wangxing@mail.buct.edu.cn (X. Wang), ligf@mail.buct.edu.cn (G. Li).
[1] These authors contributedequally to this work

https://doi.org/10.1016/j.colsurfb.2025.114757
Received 26 February 2025; Received in revised form 28 April 2025; Accepted 29 April 2025
Available online 30 April 2025

Graphene-based sponges have shown immense potential in hemostasis[32–36]. Crosslinked graphene-based sponges can absorb a droplet within 40 ms and absorb approximately 112 times their own weight in water, demonstrating exceptional liquid absorption capacity[37]. Additionally, it has been reported that the raw material, graphene oxide (GO), enhances coagulation by activating Src kinase and releasing intracellular calcium[38,39]. Furthermore, our previous studies have indicated that graphene-based sponges serve as a robust platform for anchoring guest molecules due to the unique two-dimensional lamellar structure of graphene. For example, we have developed composite sponges by immobilizing inorganic clays, such as zeolite, montmorillonite (MMT), and ophicalcite (OPH), within graphene-based sponges [40–42]. These composite sponges combine the potent clotting properties of clays with the advantage of avoiding heat-damaging of zeolite and toxic side effects of MMT and OPH. Furthermore, thrombin solution can be sprayed directly onto the surface of the graphene-based sponge, preventing the burst release of thrombin while preserving its bioactivity [43]. Consequently, graphene-based sponges offer versatility in combining with hemostatic guest molecules. This non-covalent binding strategy, however, may carry the risk of*in vivo* thrombosis due to their potential release, especially the peptides possessing strong clotting ability. Beyond safety concerns, there is a need to consider the economic aspects. The challenge lies in optimizing the graphene-based sponge platform to reduce the usage of hemostatic peptides, minimize their toxic side effects, and maximize their hemostatic properties.

Herein, a peptide-immobilized graphene/chitosan composite sponge (GCCS-TRAP) was developed for controlling severe bleeding. TRAP was successfully grafted onto a graphene/chitosan crosslinked sponge (GCCS) via thiol-ene photoclick chemistry. This light-controlled, precise immobilization method allows for controlled and stable presentation of TRAP on the sponge surface, ensuring its safe and effective hemostatic activity. The porosity, liquid absorption capacity, blood cell adsorption, and platelet activation of GCCS-TRAP were thoroughly evaluated. The hemostatic efficiency of GCCS-TRAP showed superior hemostatic performance in a rat femoral artery hemorrhage model compared to commercial hemostatic materials, such as chitosan-based powders, gelatin-based sponge, and polysaccharide-based powders. This approach provides a promising method for improving the safety and efficacy of hemostatic peptides. Moreover, the findings offer valuable insights for the design of next-generation hemostatic agents, demonstrating that light-controlled chemical immobilization can be an effective strategy for developing safer and more efficient hemostatic materials in the future.

2. Materials and methods

2.1. Materials

Chitosan was purchased from TCI Company (molecular weight is 100–200 kDa, viscosity is 5–20 mPa.s, degree of deacetylation is 75–85 %). Graphite (80 mesh) was purchased from Qingdao Jinrilai Co., Ltd., Shandong, China. Graphene oxide (GO) solution was synthesized by using the modified Hummers' method[37], and the concentration of GO solution was 10 mg/mL. Poly (ethylene glycol) diacrylate (PEGDA) was purchased from MACKLIN Company (Average molecular weight is 400). TRAP-SH (cysteine moiety with a free thiol group was engineered into the C-terminus of a TRAP6 peptide sequence, the sequence is Ser-Phe-Leu-Leu-Arg-Asn-Cys, molecular weight 743.89 Da, purity 98 %) was purchased from Nanjing Laiang Biotechnology Co., Ltd. Celox™ was obtained from Medtrade Products Ltd (Crewe, U.K.). Gelatin sponge was obtained from Hefei Qihao Medical Technology Co. Polysaccharide hemostatic powder was obtained from Shandong Sykesys Bio-technology Co. Other reagents were obtained from Sinopharm Chemical Reagent Co., Ltd., and they were used as received without any further purification.

2.2. Synthesis of methacryloylated chitosan (MAC)

The synthetic route and method of MAC[44,45] were shown in Supplementary Material (Fig. S1). The chemical structure of MAC was determined by ^{1}H spectra (Fig. S2). The degree of substitution of methacryloyl group on MAC was 28 %.

2.3. Synthesis of GCCS

GO aqueous solution and MAC aqueous solution were mixed and stirred for 3 minutes. Then, crosslinking agent PEGDA and initiator potassium persulfate (KPS) were added to the above mixed solution and stirred for 3 minutes to fully mix. The mixed solution was reacted in an oven at 70 °C for 4 hours to obtain a hydrogel. Reactant ratios are given in Table S1 of the Supplementary Data. The hydrogel was then soaked in deionized water for 24 hours to remove the unreacted portion and then freeze-dried for 48 hours to obtain the composite sponge GCCS.

2.4. Synthesis of GCCS-TRAP

A small molecule coupling agent with carbon-carbon double bond 3-(Trimethoxysilyl) propyl methacrylate (KH570) was used to construct a vinyl coating on the sponge surface. A mixed solution was prepared by adding KH570, deionized water and ethanol in the ratio of 1:1:18 into a culture flask and mixing thoroughly. The substrate sponge GCCS was placed in the mixed solution and the pH of the solution was adjusted to 4.0–4.5. The culture flask was then heated to 70 °C in a sand bath and kept for 4 hours. The sponge was then removed, washed twice with ethanol (100 mL), soaked in deionized water overnight and freeze-dried to obtain the silane coupling agent KH570 grafted sponge GCCS-KH570.

TRAP-SH was immobilized on the surface using Click chemistry. TRAP-SH was dissolved in PBS containing EDTA (pH = 8.0) with the addition of the photo initiator DMPA. The concentration of the peptide solution was 0.25 mg/mL. The sponges were immersed in this solution and irradiated for 180 s under 365 nm, 15 mW/cm^2 UV light. Subsequently, twice the volume of deionized water was added to the reaction solution and the resulting composite sponges were ultrasonically cleaned for 15 minutes to remove the clotting peptides physically adhering to the sponges. After freeze-drying for 48 h, the surface-immobilized clotting peptide composite hemostatic sponge GCCS-TRAP was obtained.

2.5. Characterization

Scanning electron microscopy (SEM, 7800) was employed to observe the inside structure. Energy-dispersive spectrometry mapping (EDS mapping, Hitachi S-4700) was used to analyze elements. Infrared spectroscopy was used to determine the changes in the functional groups before and after the reaction in order to confirm that the reaction had taken place. XPS was used to determine the Si element content on the sponge surface.

2.6. Quantitative peptide grafting amount

The Ellman's reagent method was used to determine the amount of peptide grafted[46]. Plotting standard curve: Prepare the reaction buffer by adding 1 mM EDTA to a 0.5 M PBS solution (pH 8.0). Dissolve 4 mg of DTNB in 1 mL of reaction buffer to prepare Ellman's reagent solution. Dissolve 1 mg of TRAP-SH in the prepared buffer and dilute to obtain a series of TRAP-SH standards at 1000, 500, 250, 125, 62.5, 31.25 μg/mL. Ellman's reagent solution was mixed 1:10 v/v in each standard. The UV absorbance of the reaction mixture at 412 nm was determined. A standard curve is generated from the data obtained.

Determination of peptide grafting on sponge surface: Three groups were set up. The experimental conditions for Group A were sponge immersed in a buffer solution containing TRAP-SH and subjected to UV

irradiation. Group B had the UV irradiation removed and the rest of the conditions were kept the same as that of Group A. Group C had the buffer solution containing TRAP-SH replaced with a buffer without TRAP-SH, and the rest of the conditions were kept the same as that of Group A. 100 μL sonicated solution from Group A, Group B and Group C were reacted with 10 μL of Ellman's reagent solution, and the absorbance of the solution at 412 nm was measured as $Abs_{group\ A}$, $Abs_{group\ B}$, and $Abs_{group\ C}$. The corresponding concentrations of $C_{group\ A}$, $C_{group\ B}$, and $C_{group\ C}$ were calculated from the standard curves. Peptide loading concentration = ($C_{group\ B}$ - $C_{group\ A}$ - $C_{group\ C}$) × V/S, where V represents the volume of reaction solution and S represents the area of the sponge irradiated by UV light.

2.7. Porosity measurement

The porosity of materials was measured by previously reported methods[37]. Briefly, The pre-weighed sponge (W_0) was immersed in absolute ethanol, and the saturated weight (W_1) was recorded. Porosity is calculated using the formula: Porosity = $(W_1 - W_0)/(\rho \times V)$. Among them, ρ is the density of absolute ethanol, and V is the volume of the sponge.

2.8. Liquid absorption measurement

The liquid absorption amount was measured by the weight loss method[37]. Briefly, a pre-weighed sponge (W_0) was immersed in water and recorded the saturated weight (W_1). Water absorption is calculated using the formula: Liquid absorption = $(W_1 - W_0)/W_0 \times 100$ %. The liquid absorption rate was recorded by high-speed cameras. The contact angle between the liquid and the sponge was measured by a contact angle apparatus (CA 100A).

2.9. Mechanical strength evaluation

GCCS and GCCS-TRAP are compressed at 50 % strain and are shape-fixed. The mechanical strength of the shape-fixed sponges was tested by contacting the sponges with water or blood, or by pressing the water or blood out of the sponges. The process was recorded with a digital camera to calculate the shape recovery rate and time. In addition, ten cycle stress-strain curves of GCCS and GCCS-TRAP were measured using a universal testing machine (EZ-Test, SHIMADZU).

2.10. Whole blood clotting evaluation

The blood clotting index (BCI) of materials was measured by previously reported methods[33]. Fresh citrated whole blood (CWB) was obtained from SD rat heart blood (blood: sodium citrate = 9:1). Sponge ($1 \times 1 \times 0.5\ cm^3$) was incubated with 110 μL recalcified CWB solution (100 μL CWB and 10 μL 0.2 M calcium chloride solution) and incubated for 5 minutes. Then, 25 mL DIW was added and shake at 30 rpm for 10 minutes. The absorbance value of the sample solution at 540 nm was measured (MAPADA UV-1100 spectrophotometer). DIW and PBS without added samples were used as negative and positive controls, respectively. The BCI is calculated using the formula: BCI (%) = $(Abs_{sample} - Abs_-) / (Abs_+ - Abs_-) \times 100$ %, where Abs_{sample}, Abs_+ and Abs_- value represented the absorbance values of sample, DIW and the PBS, respectively.

2.11. APTT and PT assays

The prothrombin time (PT) and activated partial thromboplastin time (APTT) were tested with MC-2000 semiautomatic coagulation analyzer (TECO, Germany). Platelet-poor plasma (PPP) was prepared by centrifuging the CWB to collect supernatant at 3000 rpm at 4 °C for 15 min[47]. Sponge powder and PPP were mixed to obtain 1 mg /mL solution. The solution to be tested was put into the detection hole of an automatic coagulation instrument for detection. The pure PPP with no added sample was used as a control.

2.12. Blood cells adhesion assays

The blood cells absorbability of materials was evaluated according to a reported method[33].

2.12.1. Red blood cells absorption

Briefly, red blood cells suspension (RBCs) was prepared by centrifuging CWB at 3000 rpm for 15 minutes. The sponge (5 mg pieces) was incubated with 100 μL RBCs at 37 ℃ for 1 hours. Free blood cells on the surface of the sponges were washed with PBS. 4 mL DIW was added to lyse RBCs and release hemoglobin for 1 hours. Samples was measured based on the absorbance at a wavelength of 540 nm. The blood cell adsorption without the sample treatment was a blank control.

2.12.2. Platelet absorption

The platelet-rich plasma (PRP) was prepared by centrifuging CWB at 1500 rpm for 5 minutes. The sponge (5 mg pieces) was incubated with 50 μL PRP at 37 ℃ for 1 hours. Free platelets on the surface of the sponges were washed with PBS. 0.6 mL of **1 %** Triton X-100 was used to lyse attached platelets for 1 hours at 37 ℃. Lysates were measured by lactate dehydrogenase (LDH) assay kit (Solarbio, China) at OD 490 nm to quantify the number of adherent platelets. The unadded sample group was used as a blank control to calculate the adsorption percentage.

2.13. Platelet activation test

Sponges were immersed in PBS and incubated at 37 ℃ for 2 hours. PRP was added to PBS at a volume ratio of 1:20, and the mixture was incubated at 37 ℃ for 1 hours. After fixing with 2.5 % glutaraldehyde solution at 4 °C for 2 hours, the samples were eluted with a series of gradient concentrations of ethanol (50 %, 60 %, 70 %, 80 %, 90 %, and 100 %) each for 10 minutes and dried. The samples were observed by SEM after spraying gold.

2.14. In vivo hemostatic properties test

This study strictly complied with the review opinions of the Laboratory Animal Welfare Ethics Committee of the Beijing Yongxinkangtai Technology Development Co. (Approval no. YXKT2024L040). All SD rats (250 ± 20 g, 7 weeks old, male) were purchased from Beijing Weitong Lihua Laboratory Animal Technology Co., Ltd. Before surgery, all rats were anesthetized with isoflurane. The vessel was completely cut off with a scalpel, and materials were applied to the arterial wound area with appropriate pressure. After the hemostasis was completed, blood loss and hemostasis time were recorded. Blank group does not use any material to stop bleeding, and the commercial hemostatic material Celox™, gelatin sponge and polysaccharide hemostatic powder were used as the control.

2.15. Biocompatibility

2.15.1. ***In vitro* hemolysis test**

The *in vitro*hemolysis test of materials was evaluated according to a reported method[41]. Washed CWB were diluted 10-fold to prepare erythrocyte suspension. The powdered sample (1 mg) was mixed with 1 mL of erythrocyte suspension. Then solutions were incubated for 1 hours at 37 °C, and centrifuged at 10000 × g for 5 minutes. The absorbance of the supernatant was measured at 540 nm. The negative control group consisted of 1 mL of red blood cell suspension, and 0.2 mL of red blood cells and 0.8 mL of DIW were mixed as the positive control group. The calculation formula of hemolysis rate was as follows: Hemolysis rate (%) = $(Abs_{sample} - Abs_+) / (Abs_- - Abs_+) \times 100$ %, where Abs_{sample}, Abs_+ and Abs_- value represented the absorbance values of

sample, DIW and erythrocyte suspension, respectively.

2.15.2. Cytotoxicity test

The cytocompatibility of materials was investigated by the extraction solution method and direct contact method using rat fibroblast cells L929 (from cell resource center, IBMS, cams/PUMC, Beijing, China). For the extraction solution method, the sample powder was added to the complete medium (CM, **90 %** RPMI-1640 medium, 10 % fetal bovine serum (FBS) and 1 % antibiotics) incubated for 24 hours to prepare 10 mg/mL leaching solution. The leaching solution was sterilized by filtration using a sterile 0.22 μm membrane filter. L929 cells were seeded in 96-well plates at a density of 5×10^4 cells/mL and pre-cultured at 37 ℃ with 5 % CO_2 for 24 hours. Then the leaching solution replaced the original medium. After an additional 24-hour incubation, 10 μL of MTT solution (3-(4,5-dimethylthiazol-2yl)-2,5-diphenyltetrazole bromide, 5 mg/mL) was added and culture for 4 hours. Cell viability was then assessed via the MTT assay at 570 nm, with biocompatibility expressed as a percentage of cell viability relative to untreated controls.

For the direct contact method, the sponge was cut into disks with 4 mm diameter and 2 mm thickness. The sponge disks were sterilized by UV irradiation and equilibrated in CM for 12 hours. L929 cells were seeded in 96-well plates at a density of 5×10^4 cells/mL and pre-cultured at 37 ℃ (5 % CO_2) for 24 hours. The sponge disks were then added to each well, ensuring that the medium level remained slightly below the sponge surface for optimal cell-sponge contact. The MTT assay was performed following the same protocol as the extraction solution method.

2.16. Statistical

All tests were processed in triplicate and similar results were acquired. Values are expressed as the means ± standard deviation (SD). Student's *t*-test was used for the treatment comparison. P-values < 0.05 were considered to be statistically significant difference. $^{ns}p > 0.05$, $*p < 0.05$, $* *p < 0.01$, $* **p < 0.001$, $* ** *p < 0.0001$.

3. Results and discussion

3.1. Synthesis and characterization of GCCS-TRAP

The preparation of GCCS-TRAP was illustrated in Fig. 1a. Firstly, MAC, GO and PEGDA were mixed to prepare GCCS. In this process, MAC and PEGDA formed crosslinked networks by thermal radical polymerization reactions. Meanwhile, GO was compounded into the crosslinked network to obtain GCCS via a ring-opening reaction between the epoxy and amine groups. Subsequently, GCCS was further modified with KH570 to introduce the olefinic double bonds. TRAP was effectively grafted onto surface of GCCS through thiol-ene photochemical click chemistry (Fig. 1b). Because GO is a carbon material that is impervious to light, TRAP was able to immobilize precisely on the surface of the sponge rather than inside. SEM images showed that GCCS-TRAP had a richly interconnected porous structure (Fig. 1c, d; Fig. S3). As shown in the FTIR spectra (Fig. 1e), intensity of the C═C stretching vibration belonging to MAC (1546 cm^{-1}) and the epoxy stretching peak of GO (860 cm^{-1}) were reduced, which proved the successful synthesis of GCCS. The stretching vibration bands at 1665 cm^{-1} appeared in GCCS-TRAP (Top), which belonged to C═O in the amide group of TRAP. According to the elemental analysis results (Fig. 1f, Table S2), the presence of the Si element in both GCCS-TRAP (Top) and GCCS-TRAP (Bot) indicated the successful modification with KH570, while the presence of the S element in GCCS-TRAP (Top) confirmed the successful grafting of TRAP. The EDS mapping (S element) results of GCCS-TRAP (Top) also confirmed the presence of TRAP (Fig. 1g; Fig. S4). The results of Elman's reagent method assay showed that the amount of grafted peptide on the surface of GCCS-TRAP (Top) was 30.62 ± 0.85 μg/cm^2 (Table S3). These results indicated the successful construction of the GCCS-TRAP network structure.

3.2. Evaluation of liquid absorption performance

The rapid liquid absorption properties of hemostatic materials, which are related to the internal structure, play a crucial role in promoting blood coagulation[37,43]. As shown inFig. 2a, the porosity of GCCS and GCCS-TRAP (Bot) is 87.9 % and 91.6 %, respectively, while the porosity of GCCS-TRAP (Top) slightly decreases to 74.2 % due to the grafting of TRAP. The high porosity of GCCS-TRAP corresponds to the porous structure observed in its SEM images. GCCS-TRAP, GCCS-TRAP (Bot), and GCCS-TRAP (Top) absorbed 36, 37, and 30 times their own weight of liquid due to their high porosity, respectively (Fig. 2b). Moreover, the GCCS could absorb a drop of liquid within 40 ms (Fig. 2c). Although the liquid absorption rate decreased due to the grafting of KH570 and TRAP, the GCCS-TRAP could still rapidly absorb the same amount of liquid within 0.27 s (Fig. 2c, d). Therefore, GCCS-TRAP was a hydrophilic material with excellent liquid absorbability. It can quickly enrich blood cells and platelets by rapidly absorbing plasma from blood, accelerating blood clotting.

3.3. Mechanical properties of GCCS-TRAP

In dealing with uncontrollable bleeding, high mechanical strength is necessary for hemostatic materials[48]. As shown inFig. 3a, both the compressed GCCS and GCCS-TRAP could retain their original shapes. Upon contact with water or blood, they quickly absorbed the liquid, allowing the sponges to restore their original form. Additionally, after 5 compression-recovery cycles, GCCS and GCCS-TRAP were still able to recover 98.3 % and 96.7 % of their original height within 1.7 s and 1.9 s in water, respectively (Fig. 3b, c, Fig. S5). Even after 10 compression-recovery cycles, GCCS and GCCS-TRAP maintain excellent recovery rates and recovery times (Fig. S6). Meanwhile, GCCS and GCCS-TRAP were able to recover 92.4 % and 93.0 % of their original height within 2.6 s and 2.8 s in the present of blood, respectively. In addition, we further investigated the mechanical strength of the material by measuring the stress-strain curve of the sponge during cyclic compression. As shown in Fig. 3d and 3e, the stresses of GCCS and GCCS-TRAP after being compressed by 50 % are 99.0 kPa and 96.3 kPa, respectively (Table S4). The stresses of GCCS and GCCS-TRAP decreased by only 10.1 % and 11.4 % after ten cycles of compression. These results demonstrate that GCCS-TRAP possesses excellent compression strength, stability, and shape recovery. The outstanding mechanical properties of the sponges are attributed to the composite structure of MAC and GO. The crosslinked network of MAC and PEGDA ensures structural stability, while GO modulates the pore structure and liquid absorption capacity, ultimately contributing to efficient rebound performance of the sponges [33,47].

3.4. In vitro coagulation properties

The blood clotting performance of the materials was evaluated using a dynamic whole blood clotting test. A lower BCI indicates a better clotting performance. As shown in Fig. 4a, the BCI for GCCS, GCCS-TRAP (Bot), and GCCS-TRAP (Top) were 23.9 %, 26.1 %, and 7.1 %, respectively. Under the clotting stimulation of TRAP, the BCI value of GCCS-TRAP (Top) decreased by 73 % compared to GCCS-TRAP (Bot), demonstrating excellent *in vitro* clotting performance. Next, the activation of the coagulation cascade pathways was tested. As shown in Fig. 4b, the Prothrombin Time (PT) values for GCCS, GCCS-TRAP (Bot), and GCCS-TRAP (Top) were 7.6 s, 7.5 s, and 7.4 s, respectively; all of them were lower than that of the control group (10.0 s). The reduction in PT values indicated the activation of the extrinsic coagulation pathway, likely due to the stimulating effect of the amino groups in chitosan. No significant difference in PT values was found between TRAP and the control group, suggesting that TRAP did not activate the

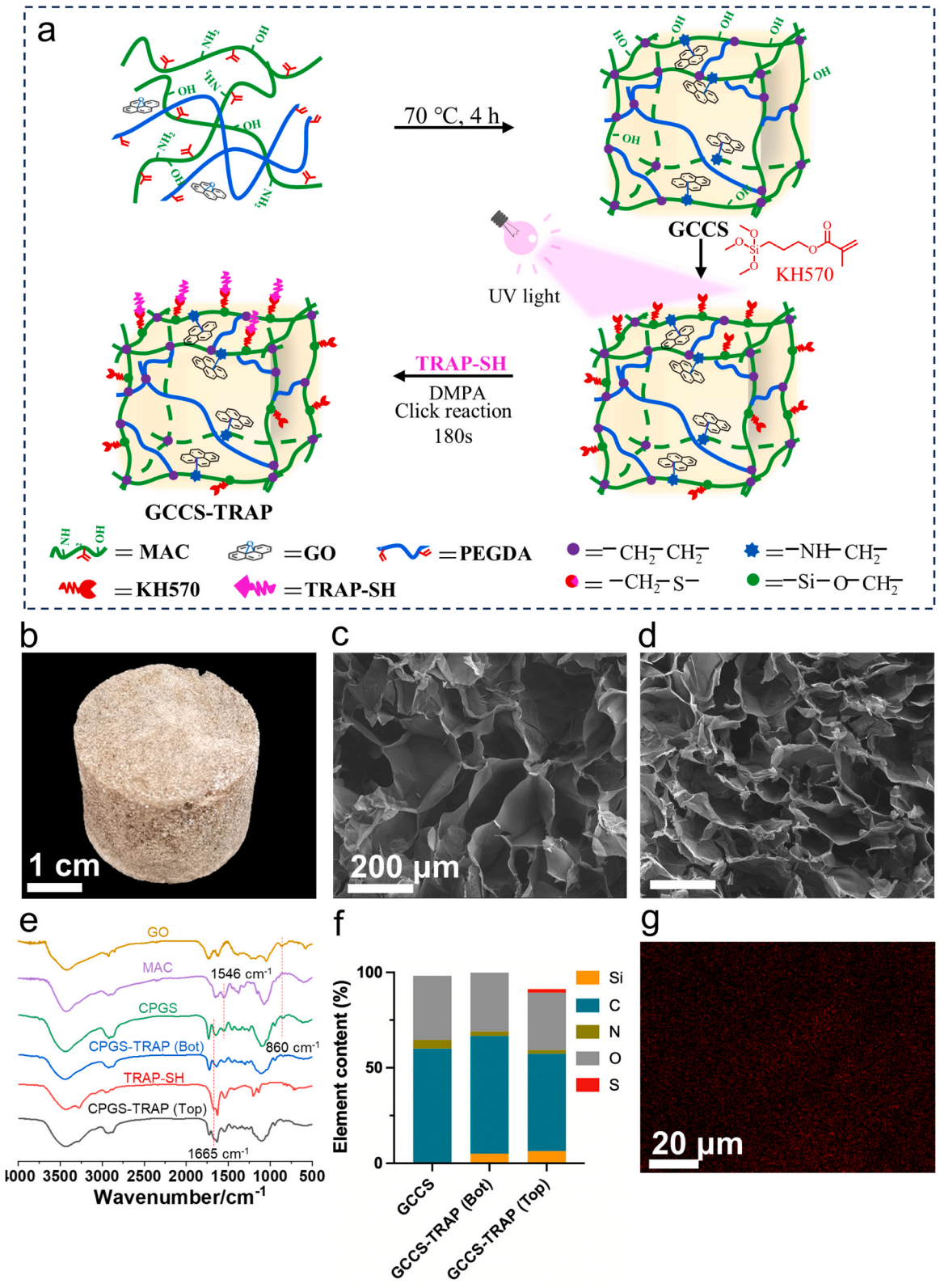

Fig. 1. Preparation of GCCS-TRAP. (a) Cartoon schematic of the GCCS-TRAP preparation; (b) photograph of GCCS-TRAP; SEM image of (c) the cross-section and (d) the longitudinal-section of GCCS-TRAP; (e) FT-IR spectra of GO, MAC, GCCS, TRAP, GCCS-TRAP (Bot) and GCCS-TRAP (Top); (f) elemental analysis of GCCS, GCCS-TRAP (Bot) and GCCS-TRAP (Top); (g) EDS mapping of S elements of GCCS-TRAP (Top). The surface within 3 mm thickness is defined as the top of the material, namely GCCS-TRAP (Top); while the other is defined as the bottom of the material, namely GCCS-TRAP (Bot).

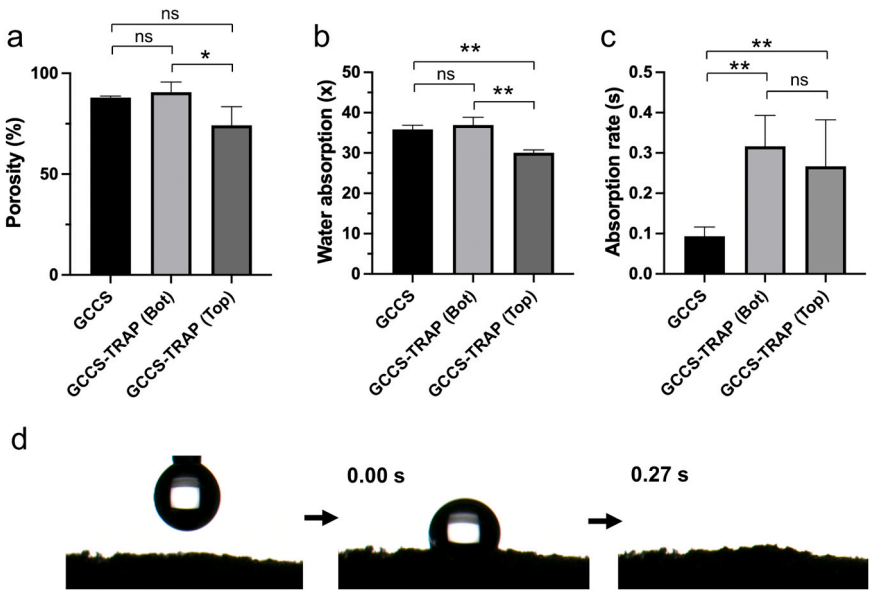

Fig. 2. Liquid absorbability of GCCS-TRAP. (a) Porosity of GCCS, GCCS-TRAP (Bot) and GCCS-TRAP (Top); (b) water absorption amount and (c) water absorption rate of GCCS, GCCS-TRAP (Bot) and GCCS-TRAP (Top); (d) dynamic water contact angle of GCCS-TRAP (Top). Error bar indicate S.D (n = 3), ^{ns} $p > 0.05$, *$p < 0.05$, * *$p < 0.01$.

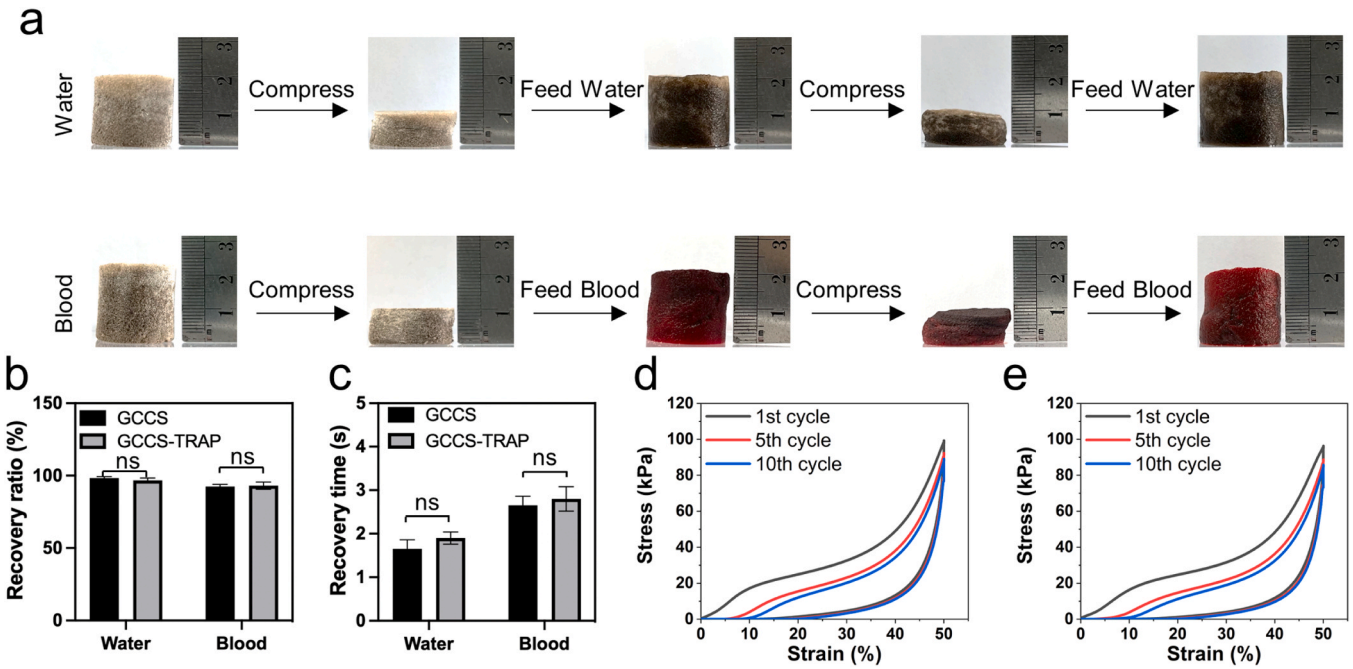

Fig. 3. Mechanical properties of GCCS-TRAP. (a) Shape memory performance of GCCS-TRAP in the presence of water or blood; (b) recovery ratio and (c) recovery time of GCCS and GCCS-TRAP within water or blood after five compression-recovery cycles; 1st, 5th and 10th cycles stress-strain curves of (d) GCCS and (e) GCCS-TRAP. Error bar indicate S.D (n = 3). ^{ns} $p > 0.05$.

extrinsic coagulation pathway. The Activated Partial Thromboplastin Time (APTT) test results (Fig. 4c) showed that the APTT values for GCCS, GCCS-TRAP (Bot), and GCCS-TRAP (Top) were 40.6 s, 41.1 s, and 40.9 s, respectively, all slightly lower than that of the control group (43.6 s). The decrease in APTT indicated the activation of the intrinsic coagulation pathway, which was attributed to the activation effect of the negatively charged carboxyl groups in GO. Therefore, GCCS-TRAP could activate both the extrinsic and intrinsic coagulation pathways, accelerating the conversion of fibrinogen to fibrin. Interestingly, TRAP alone did not activate either coagulation pathway, but GCCS, GCCS-TRAP (Bot), and GCCS-TRAP (Top) were able to activate both pathways.

The role of TRAP was to mimic thrombin function by activating the protease-activated receptor (PAR-1) signaling on platelets, leading to platelet aggregation and activation[49]. Thus, TRAP may directly activate platelet function without affecting the coagulation cascade. Therefore, we evaluated the interactions between GCCS-TRAP and red blood cells or platelets. The aggregation of red blood cells and platelets within the sponges indicated the potential for blood clotting. As shown inFig. 4d, the red blood cell adsorption rates for GCCS and GCCS-TRAP (Bot) were 47.9 % and 42.5 %, respectively. The adsorption rate of GCCS-TRAP (Top) was slightly lower at 36.6 %. Regarding platelet adsorption performance, the adsorption rates of GCCS, GCCS-TRAP

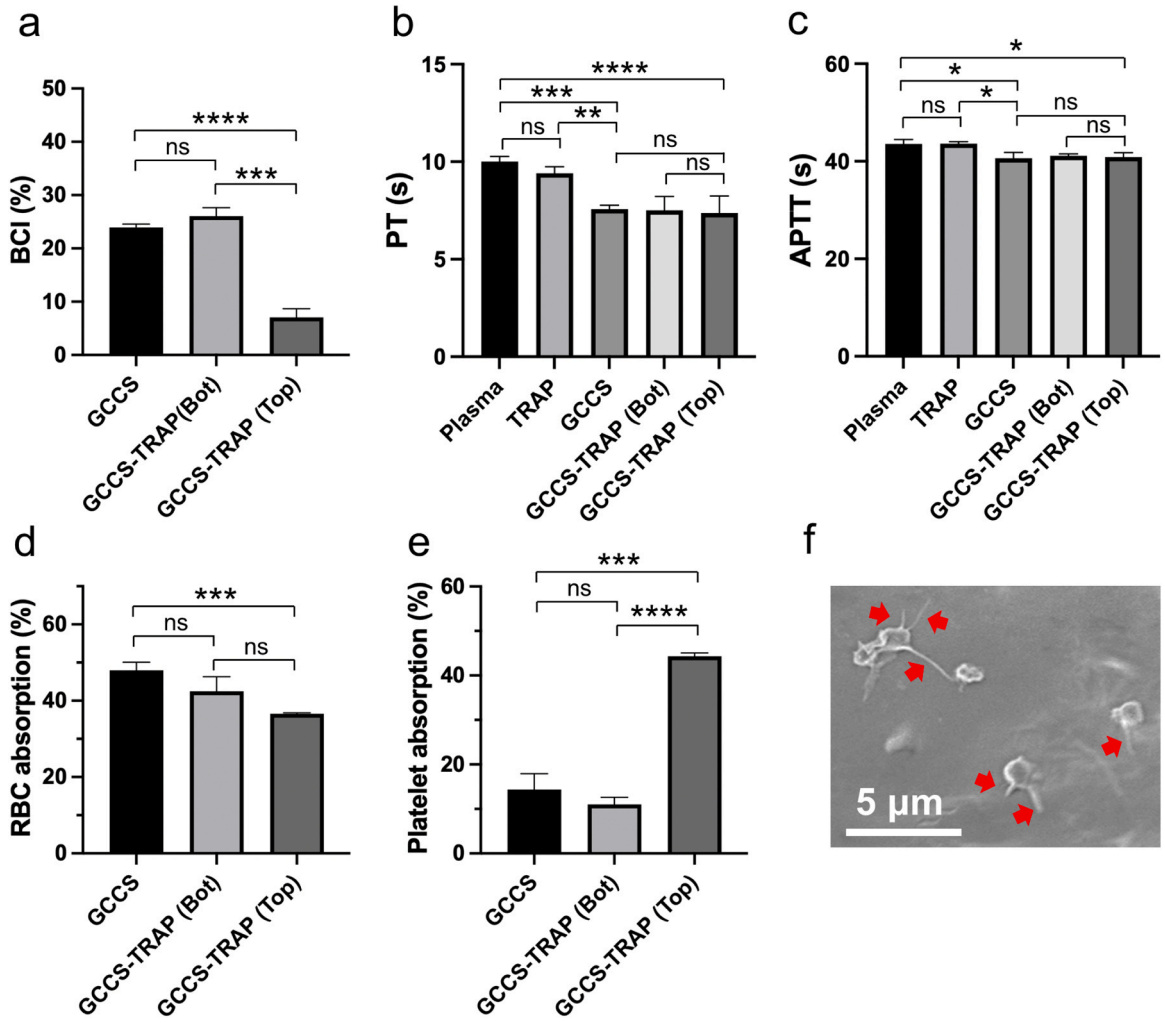

Fig. 4. *In vitro* haemostatic assays of GCCS-TRAP. (a) BCI, (b) PT and (c) APTT test of GCCS, GCCS-TRAP (Bot) and GCCS-TRAP (Top); adsorption ratio of (d) RBCs and (e) platelets in GCCS, GCCS-TRAP (Bot) and GCCS-TRAP (Top). (f) SEM images of interfacial interaction between platelets and the GCCS-TRAP (Top). Error bar indicate S.D (n = 3), ^{ns} $p > 0.05$, *$p < 0.05$, * *$p < 0.01$, * **$p < 0.001$, * ** *$p < 0.0001$.

(Bot), and GCCS-TRAP (Top) were 14.4 %, 11.0 %, and 44.3 %, respectively (Fig. 4e). Fig. S7 shows the corresponding SEM image. Significantly, the platelet adsorption rate of GCCS-TRAP (Top) was three times higher than that of GCCS-TRAP (Bot). Additionally, SEM images clearly displayed the platelets that adhered on the surface of GCCS-TRAP (Top) extended pseudopodia, indicating the activation of these platelets (Fig. 4f). These results clearly demonstrate the potent platelet aggregation and activation effects of GCCS-TRAP. Compared to both GCCS and GCCS-TRAP (Bot), GCCS-TRAP (Top) not only activates both the extrinsic and intrinsic coagulation pathways but also promotes stronger platelet aggregation and activation. Thus, the in vitro hemostatic performance of GCCS-TRAP(Top) was significantly improved, as confirmed by the reduced BCI values in the GCCS-TRAP(Top) group.

3.5. *In vivo hemostatic properties*

A rat femoral artery hemorrhage model was used to mimic massive human bleeding. Severe bleeding was induced by completely transecting the femoral artery of the rat, and the hemostatic performance of the sponges was then evaluated (Fig. 5a). Commercially available hemostats, such as chitosan hemostatic powder (Celox™), gelatin hemostatic sponges and polysaccharide hemostatic powders, were used as the positive controls. As Fig. 5b & 5c shown, the hemostatic time of GCCS was ~ 101.0 s, which was not significantly different from that of Celox™ (113.5 s). In contrast, the hemostatic time for GCCS-TRAP was 81.3 s, which represented a 54 % and 28 % reduction compared to the blank group and the Celox™, respectively. Additionally, the blood loss for GCCS was 1.69 g, which decreased of 37 % compared with that of Celox™ (2.68 g). This occurred because the powdery form of Celox™ was easily washed away by heavy bleeding, preventing it from effectively contacting the bleeding site. GCCS-TRAP possesses excellent compression strength, stability, and shape recovery. When applied to a wound, GCCS-TRAP effectively expands after absorbing blood, allowing it to better compress the wound. This ensures a close fit between the sponge and the wound, which is crucial for forming a physical barrier to promote hemostasis. Thus, the sponge form of GCCS-TRAP adhered well to the wound and rapidly absorbed fluids, accelerating the formation of a clot at the wound site. Significantly, the blood loss for GCCS-TRAP was only 1.03 g, which showed ~83 % and ~62 % reduction compared with those of the blank group and the Celox™ group, respectively. GCCS-TRAP also outperformed the other two commercial hemostatic materials, gelatin sponge and polysaccharide hemostatic powder in terms of hemostatic performance. This fully demonstrated the superior performance in stopping serious artery hemorrhage. Furthermore, the excellent mechanical strength of GCCS-TRAP ensures that it does not rupture under pressure during hemostasis, thus preventing hemostatic failure. Upon removal from the wound, the GCCS-TRAP remains intact with no residue left behind, thereby avoiding secondary injury caused by

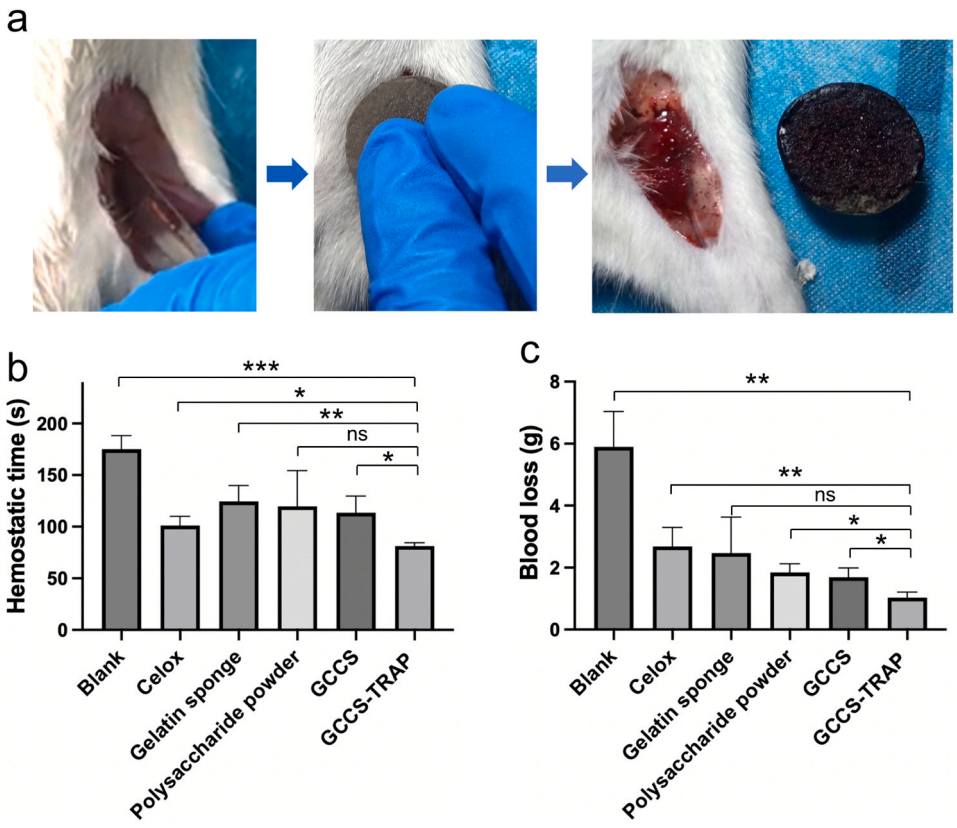

Fig. 5. *In vivo* hemostatic performance of GCCS-TRAP (a) Hemostatic process of GCCS-TRAP in SD rat artery injury model; (b) Hemostatic time and (c) blood loss of blank, Celox™, gelatin sponge, polysaccharide hemostatic powder, GCCS and GCCS-TRAP. Error bar indicate S.D (n = 5), ^{ns} $p > 0.05$, $*p < 0.05$, $**p < 0.01$, $***p < 0.001$.

residual material.

3.6. Hemostatic mechanism of GCCS-TRAP

The excellent hemostatic performance of GCCS-TRAP was attributed to the synergistic effects of rapid absorbability and strong hemostatic stimulation (Fig. 6). In terms of rapid absorbability, the GCCS-TRAP sponge contained a continuous porous structure with a high porosity of 74.2 %, which provided channels and space for blood from the wound to enter the sponge. Moreover, GO improved the hydrophilicity of GCCS-TRAP, enabling it to rapidly absorb fluids. This allowed GCCS-TRAP to quickly absorb plasma from the wound blood, thereby concentrating blood cells and forming an initial clot. The high adsorption rates for red blood cells and platelets (36.6 % and 44.3 %, respectively) further

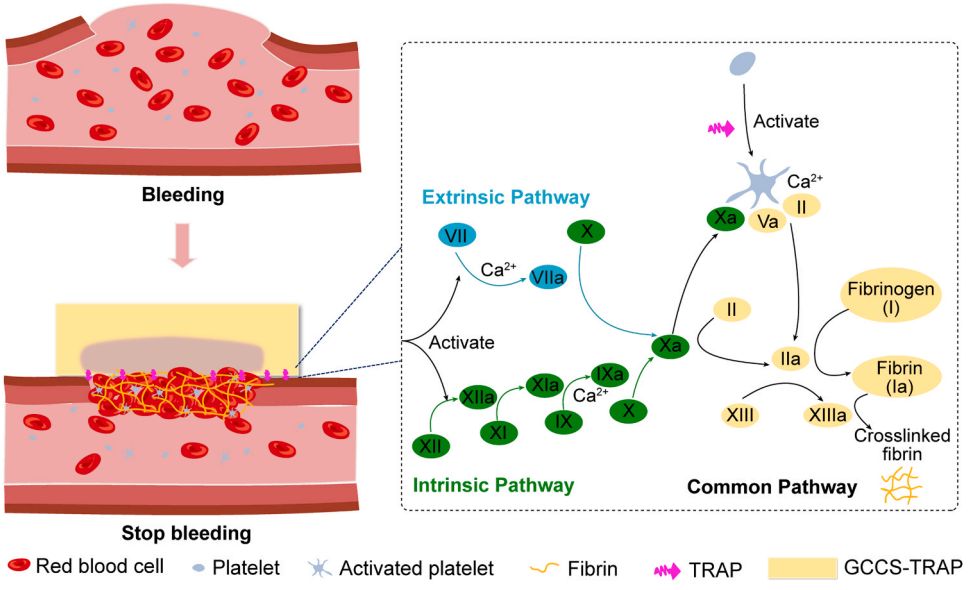

Fig. 6. Schematic diagram of hemostatic mechanism of GCCS-TRAP.

validated the strong absorbability of GCCS-TRAP.

For hemostatic stimulations, GCCS-TRAP promoted clotting by activating both platelets and the coagulation cascade pathways. First, TRAP activated PAR-1 on the surface of platelets by mimicking thrombin, leading to platelet activation. The activated platelets then underwent physical changes in their GP IIb/IIIa receptors[49], which provided high-affinity binding sites for fibrinogen. The above results promoted fibrinogen cross-linking and platelet aggregation. According to the literature, TRAP alone can promote coagulation by activating platelets, but it does not activate the extrinsic or intrinsic coagulation cascade pathways[46]. Interestingly, in our study, GCCS-TRAP activated both platelets and the coagulation cascade pathways, as evidenced by the reduction in PT and APTT values. The activation of the extrinsic coagulation pathway was likely due to the positively charged amino groups on chitosan. The intrinsic coagulation pathway was typically activated by negatively charged groups, such as carboxyl groups. GO contains abundant carboxyl functional groups, and some studies have shown that GO can activate the intrinsic pathway through negatively charged activation of Factor XII[3]. Through the combined activation of both extrinsic and intrinsic coagulation pathways, Factor X is converted into Factor Xa, triggering a cascade of reactions that ultimately result in the conversion of fibrinogen to fibrin, achieving the main goal of secondary hemostasis.

Thus, GCCS-TRAP achieved rapid hemostasis for arterial bleeding wounds through its fast liquid absorption and multiple hemostatic stimuli, including the activation of platelets and both the extrinsic and intrinsic coagulation cascades. Notably, TRAP was immobilized on the sponge surface precisely. The surface fixation strategy reinforced the interface stimulus and enhanced hemostatic effects. As a result, we reduced the amount of peptide and lowered the cost while achieving the effective hemostatic properties.

3.7. The compatibility of GCCS-TRAP

Subsequently, the compatibility of GCCS, GCCS-TRAP (Bot), GCCS-TRAP (Top), and TRAP was evaluated. As shown in Fig. 7a, the hemolysis ratios of GCCS, GCCS-TRAP (Bot) and GCCS-TRAP (Top) were 2.9 %, 3.0 % and 2.7 %, respectively. Interestingly, the hemolysis rate of GCCS-TRAP (Top) decreased from 4.0 % for TRAP to 2.7 %, indicating that TRAP was well-anchored on the surface of GCCS through the thiol-norbornene photoclick chemistry strategy, ensuring safety. Furthermore, we assessed the cytocompatibility of the materials with L929 cells. As shown in Fig. 7b, c, after 24 hours using the extraction solution method, the cell viability ratios for the GCCS, GCCS-TRAP (Bot), and GCCS-TRAP (Top) groups were 89.5 %, 97.5 %, and 104.8 %, respectively. The results of the direct contact method test showed cell viability ratios of 86.4 %, 89.0 % and 91.7 % for the GCCS, GCCS-TRAP (Bot) and GCCS-TRAP (Top) groups, respectively. There was no significant difference in cytotoxicity results at 24 and 48 hours. These results revealed the good biocompatibility of GCCS-TRAP.

4. Conclusions

In summary, we successfully developed a TRAP-grafted chitosan/graphene composite sponge (GCCS-TRAP) for efficient and rapid arterial hemostasis. The innovative use of thiol-ene photoclick chemistry allowed for the precise immobilization of TRAP onto the surface of the GCCS, ensuring controlled and stable peptide presentation. GCCS-TRAP demonstrated exceptional fluid absorption capacity and induced multiple hemostatic responses, including platelet stimulation and the activation of both the extrinsic and intrinsic coagulation cascades. In a rat femoral artery hemorrhage model, GCCS-TRAP achieved faster hemostasis and significantly reduced blood loss compared to commercially available chitosan-based hemostatic powder (Celox™), as well as polysaccharide hemostatic powders and gelatin sponges. Importantly, GCCS-TRAP showed no hemolysis or cytotoxicity, confirming its excellent biocompatibility and safety. These findings highlight that GCCS-TRAP is a highly effective and safe hemostatic material, with superior performance in arterial bleeding control, making it a promising candidate for applications in trauma care.

CRediT authorship contribution statement

Guofeng Li: Writing – review & editing, Supervision, Project administration, Funding acquisition, Conceptualization. **Xing Wang:** Writing – review & editing, Supervision, Project administration, Funding acquisition, Conceptualization. **Fang Liu:** Validation, Investigation. **Xiaojiao Pan:** Methodology, Formal analysis. **Wengjing A:** Validation, Investigation. **Muyuan Tang:** Validation, Investigation. **Fanglin Du:** Writing – original draft, Methodology, Investigation, Data curation. **Yuanhang Wang:** Methodology, Investigation, Data curation.

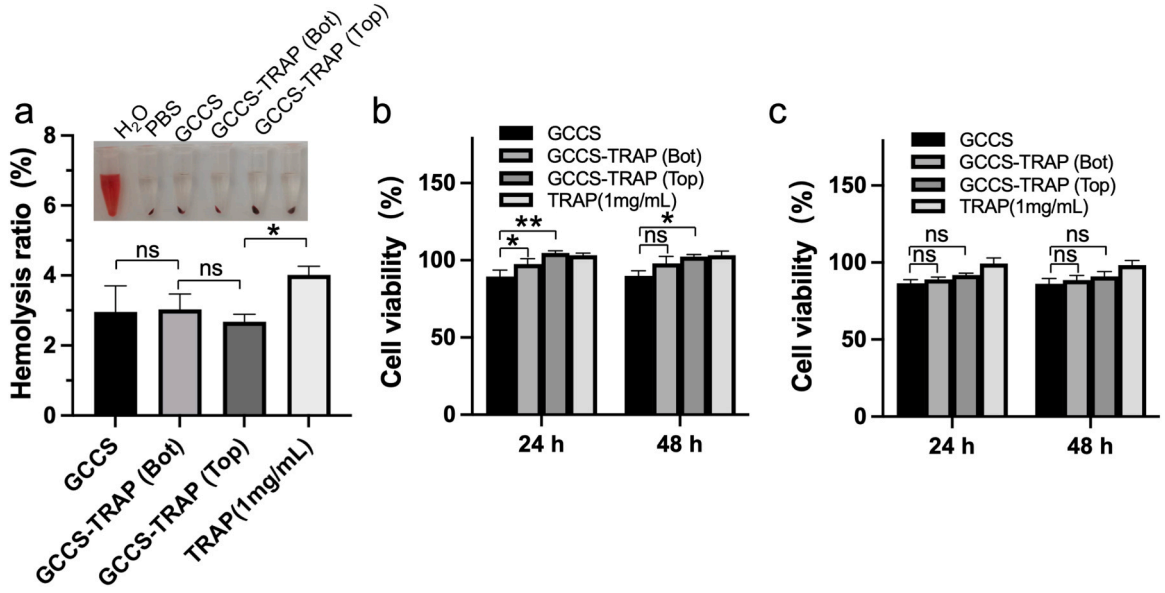

Fig. 7. (a) Hemolysis test; (b) L929 cell compatibility test using extraction solution method; (c) L929 cell compatibility test using direct contact method. Error bar indicate S.D (n = 3), ^{ns} $p > 0.05$, *$p < 0.05$, * *$p < 0.01$.

Declaration of Competing Interest

The authors declare that they have no known competing financial interests or personal relationships that could have appeared to influence the work reported in this paper.

Acknowledgments

This work was supported by the National Natural Science Foundation of China (22005020, 22275013, 52273118), the Fundamental Research Funds for the Central Universities (QNTD2023–01), and the Joint Project of BRCBC (Biomedical Translational Engineering Research Center of BUCTCJFH) (XK2023–16). G. L. thanks Baijie Liu from Beijing Yongxinkangtai Technology Development Co. for the help of the animal experiment.

Appendix A. Supporting information

Supplementary data associated with this article can be found in the online version at doi:10.1016/j.colsurfb.2025.114757.

Data availability

Data will be made available on request.

References

[1] L. Huang, G.L. Liu, A.D. Kaye, H. Liu, Advances in topical hemostatic agent therapies: a comprehensive update, Adv. Ther. 37 (2020) 4132–4148, https://doi.org/10.1007/s12325-020-01467-y.
[2] X.-F. Li, P. Lu, H.-R. Jia, G. Li, B. Zhu, X. Wang, F.-G. Wu, Emerging materials for hemostasis, Coord. Chem. Rev. 475 (2023) 214823, https://doi.org/10.1016/j.ccr.2022.214823.
[3] B. Guo, R. Dong, Y. Liang, M. Li, Haemostatic materials for wound healing applications, Nat. Rev. Chem. 5 (2021) 773–791, https://doi.org/10.1038/s41570-021-00323-z.
[4] S. Zhang, X. Lei, Y. Lv, L. Wang, L.-N. Wang, Recent advances of chitosan as a hemostatic material: Hemostatic mechanism, material design and prospective application, Carbohyd. Polym. 327 (2024) 121673, https://doi.org/10.1016/j.carbpol.2023.121673.
[5] P. Yu, W. Zhong, Hemostatic materials in wound care, Burns Trauma 9 (2021) tkab019, https://doi.org/10.1093/burnst/tkab019.
[6] Y. Guo, M. Wang, Q. Liu, G. Liu, S. Wang, J. Li, Recent advances in the medical applications of hemostatic materials, Theranostics 13 (2023) 161, https://doi.org/10.7150/thno.79639cite.
[7] X. He, Z. Xu, H. Wu, G. Sathishkumar, K. Zhang, X. Rao, M. Kharaziha, N. Li, E. Kang, L. Xu, A multimodal antibacterial platform for visualizing reactive oxygen species generation and promoting wound healing, Adv. Funct. Mater. 34 (2024) 2404708, https://doi.org/10.1002/adfm.202404708.
[8] J. Li, H. Wu, X. He, G. Sathishkumar, F. Mo, K. Zhang, M. Kharaziha, Y. Yu, E. Kang, L. Xu, Silk fibroin aerogels with AIE-featured berberine and MXene for rapid hemostasis and efficient wound healing, Int. J. Biol. Macromol. 283 (2024) 137629, https://doi.org/10.1016/j.ijbiomac.2024.137629.
[9] Y. Tan, Q. Yang, M. Zheng, M.T. Sarwar, H. Yang, Multifunctional nanoclay-based hemostatic materials for wound healing: a review, Adv. Healthc. Mater. 13 (2024) 2302700, https://doi.org/10.1002/adhm.202302700.
[10] R. Hao, X. Peng, Y. Zhang, J. Chen, T. Wang, We. Wang, Y. Zhao, X. Fan, C. Chen, H. Xu, Rapid hemostasis resulting from the synergism of self-assembling short peptide and O-carboxymethyl chitosan, ACS Appl. Mater. Interfaces 12 (2020) 55574–55583, https://doi.org/10.1021/acsami.0c15480.
[11] X. Ma, Y. Zhao, X. Jiang, M. Fan, C. He, H. Qi, Y. Wang, D. Wang, Y. Ke, H. Xu, C. Chen, J. Wang, Controlled assembly and disassembly of higher-order peptide nanotubes, ACS Appl. Mater. Interfaces (8) (2024) 9787–9798, https://doi.org/10.1021/acsami.3c17509.
[12] X. Lu, X. Li, J. Yu, B. Ding, Nanofibrous hemostatic materials: structural design, fabrication methods, and hemostatic mechanisms, Acta Bio 154 (2022) 49–62, https://doi.org/10.1016/j.actbio.2022.10.028.
[13] Q. Jiang, B. Luo, Z. Wu, B. Gu, C. Xu, X. Li, X. Wang, Corn stalk/AgNPs modified chitin composite hemostatic sponge with high absorbency, rapid shape recovery and promoting wound healing ability, Chem. Eng. J. 421 (2021) 129815, https://doi.org/10.1016/j.cej.2021.129815.
[14] P. Ding, X. Ding, X. Liu, Y. Lu, Y. Zhao, Y. Chu, L. Fan, L. Nie, Injectable, self-healing, antibacterial hydrogel dressing based on oxidized dextran and sialic acid substituted chitosan with incorporation of tannic acid, Eur. Polym. J. 216 (2024) 113297, https://doi.org/10.1016/j.eurpolymj.2024.113297.
[15] T. Ma, L. Yan, B. Wang, Q. Gong, G. Wang, T. Chen, S. Liu, H. Wei, G. He, Y. Zhang, Preparation and composition analysis of PVA/chitosan/PDA hybrid bioactive multifunctional hydrogel for wound dressing, Eur. Polym. J. 221 (2024) 113527, https://doi.org/10.1016/j.eurpolymj.2024.113527.
[16] H. Shao, X. Wu, Y. Xiao, Y. Yang, J. Ma, Y. Zhou, W. Chen, S. Qin, J. Yang, R. Wang, Recent research advances on polysaccharide-, peptide-, and protein-based hemostatic materials: a review, Int. J. Biol. Macromol. (2024) 129752, https://doi.org/10.1016/j.ijbiomac.2024.129752.
[17] Y. Xia, R. Yang, H. Wang, Y. Li, C. Fu, Application of chitosan-based materials in surgical or postoperative hemostasis, Front. Mater. 9 (2022) 994265, https://doi.org/10.3389/fmats.2022.994265.
[18] Y.K. Sung, D.R. Lee, D.J. Chung, Advances in the development of hemostatic biomaterials for medical application, Biomater. Res. 25 (2021) 1–10, https://doi.org/10.1186/s40824-021-00239-1.
[19] S. Pourshahrestani, E. Zeimaran, I. Djordjevic, N.A. Kadri, M.R. Towler, Inorganic hemostats: the state-of-the-art and recent advances, Mater. Sci. Eng. C. 58 (2016) 1255–1268, https://doi.org/10.1016/j.msec.2015.09.008.
[20] Y. Zheng, J. Wu, Y. Zhu, C. Wu, Inorganic-based biomaterials for rapid hemostasis and wound healing, Chem. Sci. 14 (2023) 29–53, https://doi.org/10.1039/d2sc04962g.
[21] S. Kattula, J.R. Byrnes, A.S. Wolberg, Fibrinogen and fibrin in hemostasis and thrombosis, Arter. Throm. Vas 37 (2017) e13–e21, https://doi.org/10.1161/atvbaha.117.308564.
[22] L.W. Chan, X. Wang, H. Wei, L.D. Pozzo, N.J. White, S.H. Pun, A synthetic fibrin cross-linking polymer for modulating clot properties and inducing hemostasis, Sci. Transl. Med. 7 (2015), https://doi.org/10.1126/scitranslmed.3010383, 277ra229-277ra229.
[23] B. Blombäck, Fibrinogen and fibrin-proteins with complex roles in hemostasis and thrombosis, Thromb. Res. 83 (1996) 1–75, https://doi.org/10.1016/0049-3848(96)00111-9.
[24] Q. Lu, J. Clemetson, K.J. Clemetson, Snake venoms and hemostasis, J. Thromb. Haemost. 3 (2005) 1791–1799, https://doi.org/10.1111/j.1538-7836.2005.01358.x.
[25] A.L. Oliveira, M.F. Viegas, S.L. da Silva, A.M. Soares, M.J. Ramos, P.A. Fernandes, The chemistry of snake venom and its medicinal potential, Nat. Rev. Chem. 6 (2022) 451–469, https://doi.org/10.1038/s41570-022-00393-7.
[26] R. Yegappan, J. Lauko, Z. Wang, M.F. Lavin, A.W. Kijas, A.E. Rowan, Snake venom hydrogels as a rapid hemostatic agent for uncontrolled bleeding, Adv. Healthc. Mater. 11 (2022) 2200574, https://doi.org/10.1002/adhm.202200574.
[27] C. Solomon, S. Traintinger, B. Ziegler, A. Hanke, N. Rahe-Meyer, W. Voelckel, H. Schöchl, Platelet function following trauma, Thromb. Haemost. 106 (2011) 322–330, https://doi.org/10.1160/TH11-03-0175.
[28] V. Evangelista, S. Manarini, G. Dell'Elba, N. Martelli, E. Napoleone, A.Di Santo, P. Savi, R. Lorenzet, Clopidogrel inhibits platelet-leukocyte adhesion and plateletdependent leukocyte activation, Thromb. Haemost. 94 (2005) 568–577, https://doi.org/10.1160/th05-01-0020.
[29] G.E. Jarvis, B.T. Atkinson, J. Frampton, S.P. Watson, Thrombin-induced conversion of fibrinogen to fibrin results in rapid platelet trapping which is not dependent on platelet activation or GPIb, Brit. J. Pharmacol. 138 (2003) 574–583, https://doi.org/10.1038/sj.bjp.0705095.
[30] M.S. Bijker, C.J. Melief, R. Offringa, S.H. Van Der Burg, Design and development of synthetic peptide vaccines: past, present and future, Expert Rev. Vaccin. 6 (2007) 591–603, https://doi.org/10.1586/14760584.6.4.591.
[31] J. White, Snake venoms and coagulopathy, Toxicon 45 (2005) 951–967, https://doi.org/10.1016/j.toxicon.2005.02.030.
[32] B. Wu, F. Du, A. Wenjing, G. Li, X. Wang, Graphene-based hemostatic sponge, Chin. Chem. Lett. 33 (2022) 703–713, https://doi.org/10.1016/j.toxicon.2005.02.030.
[33] F. Du, A. Wenjing, F. Liu, B. Wu, Y. Liu, W. Zheng, W. Feng, G. Li, X. Wang, Hydrophilic chitosan/graphene oxide composite sponge for rapid hemostasis and non-rebleeding removal, Carbohyd. Polym. 316 (2023) 121058, https://doi.org/10.1016/j.carbpol.2023.121058.
[34] X. Li, H. Cheng, X. Huang, S. Li, R. Yang, J. Wang, X. Wang, Facile construction of chitin/graphene nanocomposite sponges for efficient hemostasis, ACS Sustain. Chem. Eng. 8 (2020) 18377–18385, https://doi.org/10.1021/acssuschemeng.0c04721.
[35] G. Yang, Y. Wu, M. Liu, J. Liang, Q. Huang, J. Dou, Y. Wen, F. Deng, X. Zhang, Y. Wei, A novel method for the functionalization of graphene oxide with polyimidazole for highly efficient adsorptive removal of organic dyes, J. Mol. Liq. 339 (2021) 116794, https://doi.org/10.1016/j.molliq.2021.116794.
[36] Z. He, J. Cheng, W. Yan, W. Long, H. Ouyang, X. Hu, M. Liu, N. Zhou, X. Zhang, Y. Wei, One-step preparation of green tea ash derived and polymer functionalized carbon quantum dots via the thiol-ene click chemistry, Inorg. Chem. Commun. 130 (2021) 108743, https://doi.org/10.1016/j.inoche.2021.108743.
[37] K. Quan, G. Li, D. Luan, Q. Yuan, L. Tao, X. Wang, Black hemostatic sponge based on facile prepared cross-linked graphene, Colloid Surf. B 132 (2015) 27–33, https://doi.org/10.1016/j.colsurfb.2015.04.067.
[38] S.K. Singh, M.K. Singh, M.K. Nayak, S. Kumari, S. Shrivastava, J.J. Grácio, D. Dash, Thrombus inducing property of atomically thin graphene oxide sheets, ACS nano 5 (2011) 4987–4996, https://doi.org/10.1021/nn201092p.
[39] K. Quan, G. Li, L. Tao, Q. Xie, Q. Yuan, X. Wang, Diaminopropionic acid reinforced graphene sponge and its use for hemostasis, ACS Appl. Mater. Interfaces 8 (2016) 7666–7673, https://doi.org/10.1021/acsami.5b12715.
[40] Y. Liang, C. Xu, F. Liu, S. Du, G. Li, X. Wang, Eliminating heat injury of zeolite in hemostasis via thermal conductivity of graphene sponge, ACS Appl. Mater. Interfaces 11 (2019) 23848–23857, https://doi.org/10.1021/acsami.9b04956.
[41] G. Li, K. Quan, Y. Liang, T. Li, Q. Yuan, L. Tao, Q. Xie, X. Wang, Graphene-montmorillonite composite sponge for safe and effective hemostasis, ACS Appl.

Mater. Interfaces 8 (2016) 35071–35080, https://doi.org/10.1021/acsami.6b13302.
[42] Y. Liang, C. Xu, G. Li, T. Liu, J.F. Liang, X. Wang, Graphene-kaolin composite sponge for rapid and riskless hemostasis, Colloid Surf. B 169 (2018) 168–175, https://doi.org/10.1016/j.colsurfb.2018.05.016.
[43] G. Li, K. Quan, C. Xu, B. Deng, X. Wang, Synergy in thrombin-graphene sponge for improved hemostatic efficacy and facile utilization, Colloid Surf. B 161 (2018) 27–34, https://doi.org/10.1016/j.colsurfb.2017.10.021.
[44] L.M. Yu, K. Kazazian, M.S. Shoichet, Peptide surface modification of methacrylamide chitosan for neural tissue engineering applications, J. Biomed. Mater. Res. A 82 (2007) 243–255, https://doi.org/10.1002/jbm.a.31069.
[45] S.M. Saraiva, S.P. Miguel, M.P. Ribeiro, P. Coutinho, I.J. Correia, Synthesis and characterization of a photocrosslinkable chitosan–gelatin hydrogel aimed for tissue regeneration, Rsc Adv. 5 (2015) 63478–63488, https://doi.org/10.1039/c5ra10638a.
[46] X. Yang, W. Liu, Y. Shi, G. Xi, M. Wang, B. Liang, Y. Feng, X. Ren, C. Shi, Peptide-immobilized starch/PEG sponge with rapid shape recovery and dual-function for both uncontrolled and noncompressible hemorrhage, Acta Bio 99 (2019) 220–235, https://doi.org/10.1016/j.actbio.2019.08.039.
[47] W. A, F. Du, Y. He, B. Wu, F. Liu, Y. Liu, W. Zheng, G. Li, X. Wang, Graphene oxide reinforced hemostasis of gelatin sponge in noncompressible hemorrhage via synergistic effects, Colloid Surf. B 220 (2022) 112891, https://doi.org/10.1016/j.colsurfb.2022.112891.
[48] X. Zhao, B. Guo, H. Wu, Y. Liang, P.X. Ma, Injectable antibacterial conductive nanocomposite cryogels with rapid shape recovery for noncompressible hemorrhage and wound healing, Nat. Commun. 9 (2018) 2784, https://doi.org/10.1038/s41467-018-04998-9.
[49] X.H. Qin, K. Labuda, J. Chen, V. Hruschka, A. Khadem, R. Liska, H. Redl, P. Slezak, Development of synthetic platelet-activating hydrogel matrices to induce local hemostasis, Adv. Funct. Mater. 25 (2015) 6606–6617, https://doi.org/10.1002/adfm.201501637.